A Novel Design of High Resolution MEMS Gyroscope Using Mode-Localization in Weakly Coupled Resonators

SYED ALI RAZA BUKHARI[1], **MUHAMMAD MUBASHER SALEEM**[1,2], **(Member, IEEE), AMIR HAMZA**[1,2], **AND SHAFAAT AHMED BAZAZ**[2,3]

[1]Department of Mechatronics Engineering, National University of Sciences and Technology, Islamabad 44000, Pakistan
[2]National Centre of Robotics and Automation, Islamabad 46000, Pakistan
[3]Department of Electrical and Computer Engineering, Sir Syed CASE Institute of Technology, Islamabad 44000, Pakistan

Corresponding author: Muhammad Mubasher Saleem (mubasher.saleem@ceme.nust.edu.pk)

ABSTRACT This paper presents a novel design for a high resolution microelectromechanical systems (MEMS) technology based resonant gyroscope using the mode-localization effect in weekly coupled resonators (WCRs) as a mechanism for sensing the input angular rate. The design consists of a single proof mass with two three degree-of-freedom (3-DoF) WCRs systems attached on either side. The MEMS gyroscope is designed according to the microfabrication constraints of the foundry process, silicon-on-insulator multi-user MEMS process (SOIMUMPs). The shift in the resonance frequency values, amplitude ratios of the WCRs, and amplitude ratios difference of two sets due to electrostatic stiffness perturbation, corresponding to the input angular rotation, are discussed as an output metric for the measurement of angular rate. The results show that the amplitude ratio difference as an output metric allows achieving a linear output response and large dynamic range in comparison to the shift in the amplitude ratio and resonance frequency in 3-DoF WCRs in a single set. The dynamic range and resolution of the MEMS gyroscope in terms of maximum allowed resonators amplitude and the noise floor is discussed. The proposed MEMS gyroscope design has a sensitivity of 62830 ppm/°/s based on a difference in the amplitude ratios of resonators in two 3-DoF WCRs systems and a dynamic range of ± 100 °/s. The resolution of the MEMS gyroscope is 31.09×10^{-6}°/s which is significantly higher than existing MEMS gyroscopes and is comparable to traditional bulky ring laser gyroscopes. This high resolution makes the proposed MEMS gyroscope design suitable for use in applications such as earth rotation rate measurement for gyrocompassing and high precision robotics.

INDEX TERMS Amplitude ratio, finite-element-method (FEM), MEMS, microfabrication process, MEMS gyroscope, mode-localization, resolution, sensitivity, weakly coupled resonators.

I. INTRODUCTION

MEMS based sensors have applications in many areas due to their small size, lower cost due to batch fabrication, and ease of integration with integrated circuit (IC) technology [1], [2]. Particularly, MEMS gyroscopes have found a wide range of applications in consumer electronics, navigation systems, and the automotive industry [3]–[5].

MEMS gyroscopes can be divided into two distinct categories, resonant and non-resonant gyroscopes, based on

The associate editor coordinating the review of this manuscript and approving it for publication was Salvatore Surdo.

their mode of operation. The resonant MEMS gyroscopes operate at resonant frequencies and utilize the phenomenon of mode matching between the drive and sense modes to achieve high sensitivity and resolution. The non-resonant MEMS gyroscopes operate in the area between the resonance peaks where the vibration amplitude of oscillating masses remains constant for a given frequency bandwidth. Thus, non-resonant MEMS gyroscopes inherently show robustness against any frequency change due to microfabrication process tolerances and environmental variations [6], [7]. However, this robustness is a trade-off with the sensitivity, as the sensitivity of non-resonant MEMS gyroscopes is lower due

to operation in the flat region between two resonant peaks where the oscillation amplitude is low. To increase the oscillation amplitude in non-resonant MEMS gyroscopes, different approaches based on the dynamic amplification have been implemented [8]–[10], but the sensitivity and resolution of the non-resonant MEMS gyroscopes are generally low compared to resonant MEMS gyroscopes.

The mode matching in the resonant MEMS gyroscopes allows to achieve high sensitivity, but the low gain away from the resonance frequency and narrow bandwidth are major concerns for such devices. To resolve these issues, additional error compensation circuitry and structural modifications are required [11]–[13]. One of the most commonly used techniques to eliminate the mismatch between the resonant frequencies of drive and sense mode is the use of the electrostatic spring softening effect [14]. Real time mode matching has also been proposed such that if the frequencies of the operational modes shift during operation, the frequency tuning voltage can be changed to achieve continuous mode matching [15], [16]. In addition to the sensitivity, the resolution also plays an important role in deciding the application areas where MEMS gyroscopes can be used. In the case of resonant MEMS gyroscopes, the resolution of the device is highly dependent on the displacement sensitivity, transduction mechanism, and readout circuitry. A mismatch between the modes can lead to low sensitivity and hence low resolution whereas, using high resolution circuitry can increase the cost of the device and is thus not a viable solution. The limited resolution of the resonant MEMS gyroscopes has limited their applications in applications requiring high resolution such as earth rate measurement and high precision robotics. Although some MEMS gyroscopes have been developed for high resolution applications like earth rotation rate measurement but they have high error rates and require complex control systems to work as intended [17], [18].

Generally, a mode localized system consists of multiple weakly coupled resonators (WCRs). The concept of mode-localization involves the confinement of energy into any one of the resonators due to an input stiffness perturbation in the coupled resonator system. The corresponding changes in the amplitude response or the resonant frequencies of the resonators can then be used as the output metric for the physical parameter to be measured. Mode localization has recently been adopted in the design of ultrasensitive MEMS sensors for the measurement of quantities such as force, mass, and acceleration [19]–[21]. MEMS gyroscopes can also benefit from the enhanced sensitivities by using mode localization which can enable them to be used in high resolution applications such as earth rotation measurement and high precision robotics [17], [22]. In the case of MEMS gyroscopes, the induced Coriolis force as a result of the applied angular rate can be used as the perturbing factor for the resonator system and the output metric of frequency or amplitude change can be used to measure the applied angular rate.

The frequency shift in the weakly coupled resonators as a measure of the input quantity is susceptible to performance loss due to environmental fluctuations and is limited by the type of materials used for fabrication [23]. Another output metric for measuring the input quantity using mode localization in WCRs is the amplitude ratio of the resonators [24]. Initially, the amplitudes of the resonators kept the same which results in an amplitude ratio (AR) of 1 but as the mechanical stiffness of one of the resonators is perturbed, the resonators amplitude and hence the AR changes. This change in the AR is thus used to measure the input quantity. Generally, two weakly coupled resonators are used for utilizing the mode localization effect [23], [24] but the sensitivity of such sensors is limited. In [25], a three weakly coupled resonators based MEMS sensor has been presented to achieve higher sensitivity.

A major issue with using the amplitude ratio of the mode localized WCRs as an output metric for the input is the inherent nonlinearity for low input values. This is undesired as low input values cannot be measured accurately. Additionally, the amplitude ratio of the WCRs reduces drastically when the direction of applied input changes from positive to negative and vice versa. To overcome this, systems utilizing the amplitude ratio difference (ARD) by using two sets of WCRs arranged in a differential configuration have been recently presented [20], [26] where two sets of WCRs are attached on either side of the central proof mass and difference of the amplitude ratios of the WCRs in the individual sets is used an output metric for low g acceleration measurement which provides a linear output response throughout the input acceleration measurement range. In this paper, a novel design of high resolution resonant MEMS gyroscope using mode localization in 3-DoF WCRs and amplitude ratio difference as an output metric for input angular rate measurement for the applications including earth rate measurement and precision robotics is presented. The proposed MEMS gyroscope design allows achieving higher sensitivity and resolution in comparison to the conventional resonant MEMS gyroscopes.

II. STRUCTURAL DESIGN OF THE RESONANT MEMS GYROSCOPE

Fig. 1 shows the design scheme of the proposed MEMS gyroscope design utilizing mode localization in the WCRs as a sensing mechanism for input angular rate. The gyroscope design is constructed around a central proof mass which is connected to the rest of the structure through mechanical springs. The mechanical design mainly consists of five distinct parts including proof mass, drive frames, sense frames, resonator Set A and resonator Set B. The proof mass is connected to the drive and sense frames through a pair of double folded serpentine shaped mechanical springs. The mechanical structure of the springs and decoupling frames in the gyroscope design allows to minimize the cross-axis coupling.

The proof mass is electrostatically driven into resonance by using the comb drive-based actuator. The displacement amplitude of the proof mass in the drive axis is designed to be measured by using displacement sensing combs attached
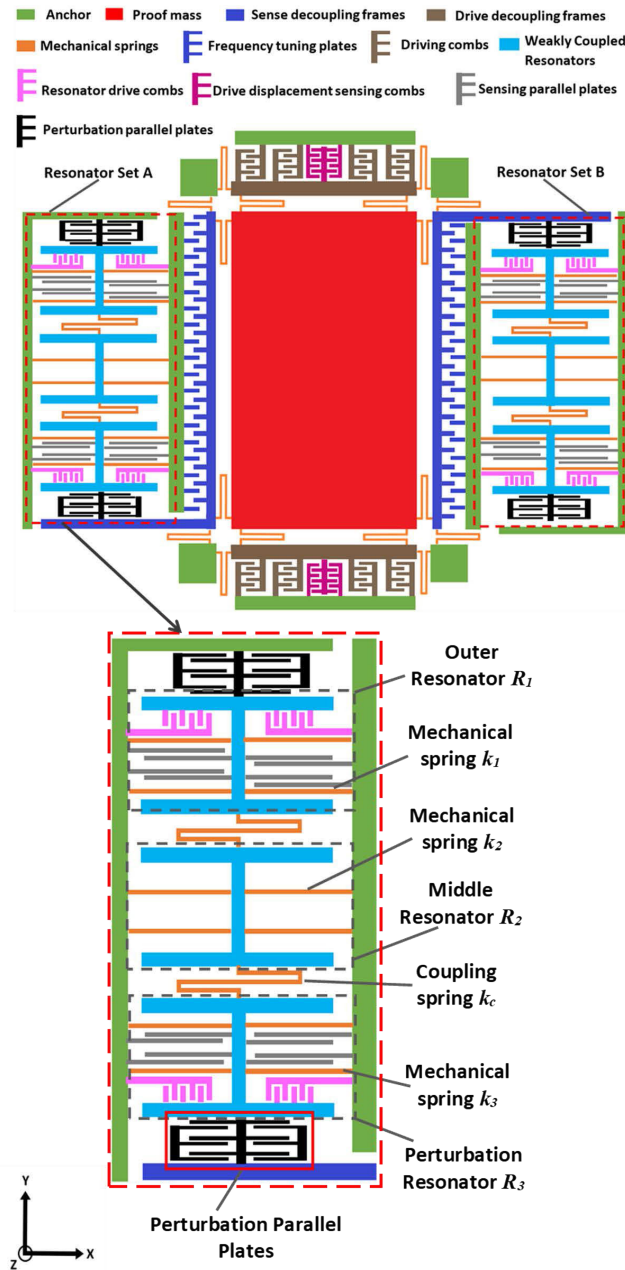
FIGURE 1. Schematic of the proposed mode localization based resonant MEMS gyroscope design.

using electrostatic comb drives and their oscillation amplitude is designed to be measured utilizing parallel capacitive plates. The displacement of the proof mass due to Coriolis force results in an electrostatic stiffness perturbation in both the WCRs sets through perturbation parallel plates. This results in mode-localization and amplitude ratio of the outer resonators in any of the two resonator sets or difference between the amplitude ratios of the outer resonators in resonator Set A and Set B can be used as an output metric for the proof mass displacement measurement and hence the input rotation. The perturbation parallel sensing plates are attached to the opposite outer resonators in the two resonator sets. When the proof mass moves in the sense direction (y-axis), after the application of an angular rate, the electrostatic gap between the perturbation parallel plates in the resonator Set A increases and in Set B it decreases. This way the two resonator systems on the right and left sides of the proof mass form a differential system. Table 1 shows the design parameters and their values for the proposed MEMS gyroscope design.

TABLE 1. Important Design Parameters for the MEMS Gyroscope.

Design Parameters	Values
Overall size	4.35 mm × 4.35 mm
Silicon layer thickness (t)	25 µm
Mass (m_x)	3.5702×10^{-7} Kg
Mass (m_y)	3.4767×10^{-7} Kg
Resonator R_1 mass (m_1)	1.45187×10^{-8} Kg
Resonator R_2 mass (m_2)	1.39688×10^{-8} Kg
Resonator R_3 mass (m_3)	1.45187×10^{-8} Kg
Perturbation parallel plates length (l)	100 µm
Perturbation parallel plates width (w)	3 µm
Overlapping length of perturbation parallel plates (l_0)	90 µm
Small gap size of perturbation parallel plates (d)	8 µm
Number of perturbation parallel plate pairs (N)	8
Number of combs pairs in comb drive actuators (N_D)	392
Drive comb width (w_D)	3 µm
Drive comb length (l_D)	40 µm
Gap size between the drive combs (d_D)	4.5 µm

to the proof mass. For the drive and sense mode frequency matching, electrostatic frequency tuning parallel plates are attached to both of the sense decoupling frames. For a rotation in the z-axis, a Coriolis force is generated in the y-axis i.e. axis perpendicular to both the driving and rotation axis. The displacement in the proof mass, corresponding to developed Coriolis force, is sensed by using the 3-DoF WCR systems (resonator Set A and B) attached on both sides of the central proof mass. Each resonator set consists of three weakly coupled H-shaped resonators through mechanical springs and anchored to the substrate through fixed-fixed mechanical beams. The two outer resonators are actuated at resonance by

A. MICROFABRICATION PROCESS AND DESIGN CONSTRAINTS

The design of the MEMS gyroscope design is optimized according to the constraints of the foundry process SOIMUMPs by MEMSCAP Inc. USA [27]. This process allows to develop high aspect ratio MEMS devices with a structural layer of Silicon. The SOIMUMPs process consists of a single wafer with 4 main layers namely the padmetal layer of 0.52 µm thickness, the silicon structural layer with a thickness of 25 µm, the oxide layer with a thickness of 2 µm, and a silicon substrate with 400 µm thickness. Fig. 2 shows the main microfabrication steps for the MEMS gyroscope.

Initially, a silicon-on-insulator wafer is doped with a phos-phosilicate glass layer (PSG layer) followed by annealing at a temperature of 1050 °C in Argon. The PSG layer is then removed using wet etching. A 0.52 μm thick pad metal layer, consisting of 20 nm thick chromium and 500 nm thick gold, is then deposited by using a lift-off process (Fig. 2(b)). The silicon layer is patterned using a second mask and photolithography. Finally, a trench mask is applied on the substrate which is patterned using a lithography technique in conjunction with the successive deep – reactive – ion – etching (DRIE) process (Fig. 2(d)).
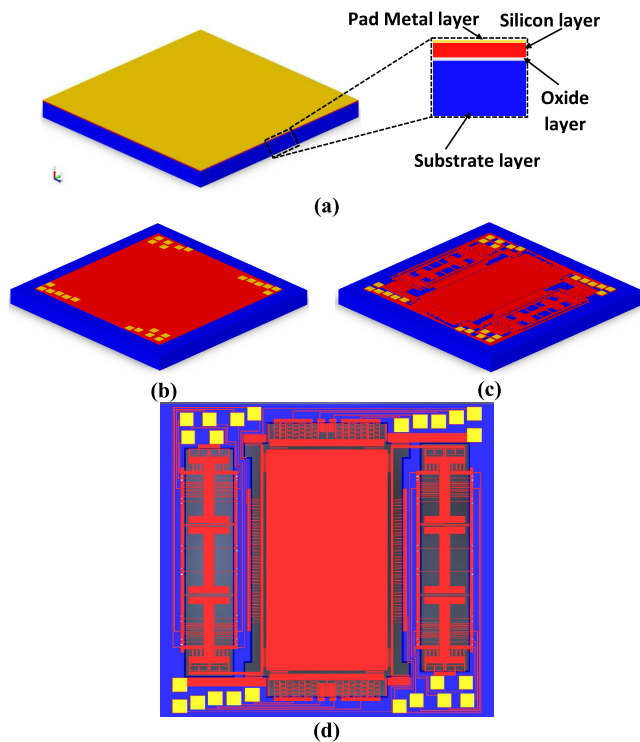
FIGURE 2. Steps for the microfabrication process of the proposed MEMS gyroscope design.

The SOIMUMPs microfabrication process has some design rules which must be followed for the successful fab-rication of the device. These rules impose limitations that prevent the use of some features in the design. The first limitation is that the design cannot have anchors which are surrounded by moving structures from all sides. The second limitation is due to the absence of the bottom electrode as the substrate is completely etched through. The third main limitation is that the etched area of the silicon structural layer should be less than 33% of the total area.

The proposed MEMS gyroscope design is optimized by following these microfabrication process constraints while keeping the overall structure simple. The resonator sets A and B need to be anchored from both sides as shown in Fig. 1. For providing the anchor to the resonator sets, the sense decoupling frame is made to be unsymmetrical such that the anchor can be connected to the fixed structure around

the periphery of the device. Since out of plane proof mass displacement is not possible with the SOIMUMPs process so, the drive and sense axes are kept in-plane, and the input angular rate is along the z-axis. The final limit concerns with the etched area of the structural layer, thus to minimize the etched area the proof mass in the center is considerably large and the empty spaces in the design are kept minimum.

III. ANALYTICAL MODELING FOR THE MEMS GYROSCOPE

A. MEMS GYROSCOPE DYNAMICS

Fig. 3 (a) and (b) show the mass-spring-damper model of the main MEMS gyroscope structure and 3-DoF WCR based sensing structure respectively. The proof mass along with drive and sense decoupling frames is suspended through serpentine mechanical springs with drive and sense direction stiffness of k_x and k_y respectively. The air damping force acting on the proof mass in the drive axis, due to slide film damping and in the sense axis due to squeezed film damping, is represented by the damping coefficients c_x and c_y respectively.
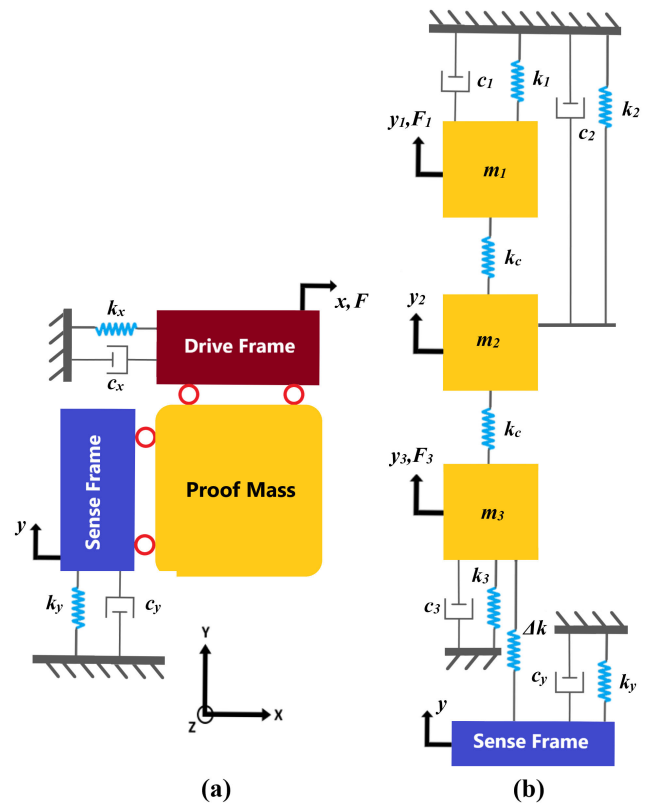

FIGURE 3. Mass-spring-damper model of the MEMS gyroscope design (a) The proof mass system and (b) the resonator system.

The equations of motion for the proof mass and decoupling frames are given as;

$$m_x\ddot{x} + c_x\dot{x} + k_x x = F cos(\omega t) \tag{1}$$

$$m_y\ddot{y} + c_y\dot{y} + k_y y = F_c \tag{2}$$

where F_c is the Coriolis force acting on the system and is given as $F_{c(m_{3a})} = -2m_y\Omega\dot{x}$, m_x and m_y are the combination of the proof mass and respective decoupling frame masses in the drive and sense axis respectively. The electrostatic force acting on the proof mass in the drive axis is given as [28];

$$F_D = 4\frac{\varepsilon_0 t N_D}{d_D}V_{DC}v_{AC} \tag{3}$$

where ε_0 is the permittivity, t is the thickness of combs, N_D is the number of fixed and moving comb pairs, d_D is the gap between the combs, V_{DC} is the applied DC voltage and v_{AC} is the applied AC voltage. The 3-DoF WCRs based system consists of three resonators with mass m_1, m_2 and m_3 where m_1 and m_3 are connected to the mass m_2 through coupling mechanical spring k_c. The three resonators, in a single resonator set, are suspended and anchored to the fixed supports through mechanical springs represented by k_1, k_2 and k_3 in Figure 3(b). The F_1 and F_3 represent the electrostatic actuation force on the outer resonators. The electrostatic stiffness perturbation Δk due to proof mass displacement in the sense axis results in overall stiffness change in the resonator electrostatically coupled to the proof mass in both resonator Set A and Set B. The final stiffness of the resonator is thus $k_3' = k_3 + \Delta k$. The equations of motion for the three resonators in the resonator set A, can be written as;

$$[M]\ddot{Y} + [C]\dot{Y} + [K]Y = [F] \tag{4}$$

$$\begin{bmatrix} m_1 & 0 & 0 \\ 0 & m_2 & 0 \\ 0 & 0 & m_3 \end{bmatrix}\begin{bmatrix} \ddot{y}_1 \\ \ddot{y}_2 \\ \ddot{y}_3 \end{bmatrix} + \begin{bmatrix} c_1 & 0 & 0 \\ 0 & c_2 & 0 \\ 0 & 0 & c_3 \end{bmatrix}\begin{bmatrix} \dot{y}_1 \\ \dot{y}_2 \\ \dot{y}_3 \end{bmatrix}$$

$$+ \begin{bmatrix} k_1 + k_c & -k_c & 0 \\ -k_c & k_2 + 2k_c & -k_c \\ 0 & -k_c & k_3' + k_c \end{bmatrix}\begin{bmatrix} y_1 \\ y_2 \\ y_3 \end{bmatrix}$$

$$= \begin{bmatrix} F_1 cos(\omega t) \\ 0 \\ F_3 cos(\omega t) \end{bmatrix} \tag{5}$$

The solution for this system can be written as;

$$[X] = [A]\sin(\omega t) + [B]cos(\omega t) \tag{6}$$

where $[A] = \begin{bmatrix} a_1 \\ a_2 \\ a_3 \end{bmatrix}$ and $[B] = \begin{bmatrix} b_1 \\ b_2 \\ b_3 \end{bmatrix}$ whereas, a_i and b_i represent the solution of the equations for the three resonator system. Using this solution in the equation above we get;

$$[T]\begin{bmatrix} [A] \\ [B] \end{bmatrix} = \begin{bmatrix} [F] \\ [0] \end{bmatrix} \tag{7}$$

And;

$$[T] = \begin{bmatrix} [K] - \omega^2[M] & -\omega[C] \\ \omega[C] & [K] - \omega^2[M] \end{bmatrix} \tag{8}$$

The oscillation amplitude of the resonators can thus be written as;

$$y_i(\omega) = \sqrt{A_i + B_i} \tag{9}$$

$$tan\theta_i = -\frac{B_i}{A_i} \tag{10}$$

where i shows the resonator for which the calculations are being carried out.

In this work, the amplitude ratio $AR_{SetA} = {y_1}/{y_3}$ and $AR_{SetB} = {y_4}/{y_6}$ of the outer resonators in resonator Set A and B respectively and amplitude ratio difference $|AR_{SetA} - AR_{SetB}|$ of the outer resonators in two sets is discussed as an output metric for the angular rate measurement. With the assumptions that there is negligible damping in coupled resonators, the mechanical stiffness of outer resonators in the resonator Set A is equal i.e. $k_1 = k_2 = k$, the masses of the three resonators are identical i.e., $m_1 = m_2 = m_3 = m$ and the electrostatic perturbation stiffness is much less than the overall stiffness of the resonator i.e., $\Delta k \ll k_3'$, the first two mode frequency for 3-DoF WCRs based system in the resonator Set A can be written as [25];

$$\omega_{ip}$$
$$= \sqrt{\frac{1}{m}\left[k + k_c + \frac{1}{2}\left(\Delta k - \frac{2k}{\gamma} - \sqrt{\Delta k^2 + \left(\frac{2k}{\gamma}\right)^2}\right)\right]} \tag{11}$$

$$\omega_{op}$$
$$= \sqrt{\frac{1}{m}\left[k + k_c + \frac{1}{2}\left(\Delta k_3 - \frac{2k}{\gamma} + \sqrt{\Delta k^2 + \left(\frac{2k}{\gamma}\right)^2}\right)\right]} \tag{12}$$

here ω_{ip} and ω_{op} represent the in-phase and out-of-phase modal frequencies respectively. The term γ in the above equation can be written as;

$$\gamma = \frac{k[k_2 - k + k_c]}{k_c^2} \tag{13}$$

B. MECHANICAL STIFFNESS CALCULATION

The mechanical stiffness in the drive and sense direction for the proof mass and the decoupling frames can be found by modeling the serpentine shaped mechanical springs as fixed guided beams and is given as;

$$k_x = \frac{8}{2}\left(\frac{12EI}{L_{k_x}^3}\right) = \frac{4Etw_{k_x}^3}{L_{k_x}^3} \tag{14}$$

$$k_y = \frac{8}{2}\left(\frac{12EI}{L_{k_y}^3}\right) = \frac{4Etw_{k_y}^3}{L_{k_y}^3} \tag{15}$$

where L_{k_x} and w_{k_x} are the lengths and widths of the serpentine mechanical springs, E is the Young's Modulus of silicon structural layer, $I = \frac{wt^3}{12}$, and w and L represent the width and length of the spring k_i with t as the thickness. The mechanical suspension beams attached to three resonators in the resonator Set A and Set B can be modeled as fixed-fixed

microbeams and their stiffness is given as;

$$k_i = 4 \left(\frac{48EI}{L_{k_i}^3} \right) = \frac{16Etw_{k_i}^3}{L_{k_i}^3} \qquad (16)$$

where w_{k_i} and L_{k_i} are the width and length of the suspension beams in the ith resonator. The coupling mechanical spring between the middle resonator and two outer resonators in the 3-DoF resonator set can be modeled as a fixed guided beam and its overall stiffness can be calculated as;

$$k_c = \frac{1}{4} \left(\frac{12EI}{L_{k_y}^3} \right) = \frac{Etw_{k_c}^3}{4L_{k_c}^3} \qquad (17)$$

here w_{k_c} and L_{k_c} are the width and length of the mechanical coupling spring beams.

C. ELECTROSTATIC STIFFNESS PERTURBATION

The stiffness perturbation is introduced in the WCRs in resonator Set A and Set B due to displacement of the sense decoupling frame corresponding to input rotation which is electrostatically coupled to the resonator system using the perturbation parallel plates. The movement of the sense decoupling frame changes the gap between the perturbation parallel plates, resulting in a change in the electrostatic stiffness (Δk). By considering the resonator Set A the effective stiffness of resonator R_3 can be written as k_3' [28];

$$k_3' = k_3 + \Delta k \qquad (18)$$

$$\Delta k = -\frac{N\varepsilon A}{\left(d + \frac{F_c}{k_y} - \frac{F_c}{k_3} + y_g \right)^3} (\Delta V)^2 \qquad (19)$$

where N is the total number of perturbation parallel plate pairs, Δk represents the stiffness perturbation, ΔV is the applied potential difference between the perturbation parallel plates and F_c is the induced Coriolis force experienced by the sense decoupling frame after the application of an angular rate. The term y_g in (19) is derived by rearranging the electrostatic stiffness equation. It represents the initial displacement due to the applied potential across the perturbation parallel plates and can be modeled as;

$$y_g = \frac{0.5\varepsilon_0 A (\Delta V)^2}{k_y} \left(\frac{1}{\left(d - \frac{F_c}{k_y} \right)^2} - \frac{1}{\left(d + \frac{F_c}{k_y} \right)^2} \right) \qquad (20)$$

where A is the overlap area of the perturbation parallel plates and d is the gap between them, k_y represents the stiffness in the sense direction.

A FEM analysis is performed to find the sensitivity of the change in stiffness of the perturbed resonator to the applied angular rate. The value of air damping for the system at room temperature and operating pressure of 10 mTorr is found using the DampingMM module of CoventorWare Analyzer. Initially, the stiffness of the mechanical spring k_3' is 52 N/m, which is reduced to 51.7 N/m after the initial biasing of the resonators. Afterward, displacement in the perturbation parallel plates further reduces the stiffness of k_3'. The change

in the overall stiffness of resonator R_3 for an applied angular rate in the range of ± 50 °/s is shown in Fig. 4. The results show that the stiffness perturbation ($\Delta k/k$) remains nearly linear in this range. The stiffness perturbation values increase for resonator Set A whereas they decrease for the resonator Set B. This can be attributed to an increase in the gap between the perturbation parallel plates for resonator Set A and a simultaneous decrease in the gap for Set B. The stiffness perturbation sensitivity is found to be 0.00198 $(N/m)/(°/s)$.
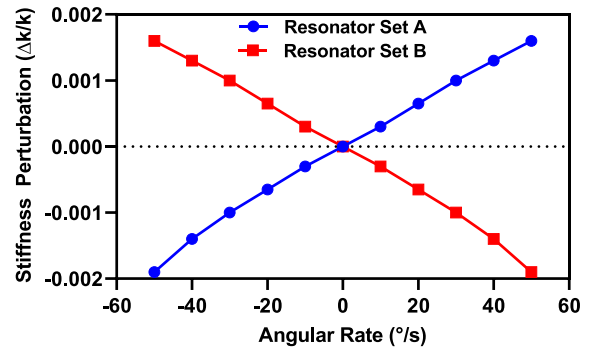

FIGURE 4. Stiffness perturbation in the resonators electrostatically coupled to proof mass for an angular rate of ± 50 °/s.

IV. FEM ANALYSES OF THE MODE LOCALIZATION BASED RESONANT MEMS GYROSCOPE

A. MODAL ANALYSIS

The drive and sense mode natural frequency values and corresponding mode shapes for the proof mass system and electrostatically coupled 3-DoF WCRs system are obtained through FEM simulations in the CoventorWare software. In the analysis, the density of 2500 kg/m³, Young's Modulus of 169 GPa, and Poisson ratio of 0.29 are used for the silicon structural layer [10]. Fig. 5 (a) and (b) show the drive and sense mode shapes for the MEMS gyroscope with resonant frequency values of 2832.46 Hz and 2892.78 Hz respectively. These values are close to the mathematically calculated values of 2871.314 Hz and 2960.695 Hz for the drive and sense modes respectively. The results show that at these resonant frequency values, only proof mass and decoupling frames move in the desired direction while displacement in the 3-DoF WCRs is negligible. The initial resonant frequency mismatch between drive and sense modes is 60.3 Hz with a higher frequency value for the sense mode. This is to compensate for the frequency difference between the two modes owing to microfabrication process tolerances and operating temperature variations.

Fig. 6 (a) and (b) show the out-of-phase and in-phase mode shapes of 3-DoF weakly coupled resonator system with resonant frequency values of 9416.48 Hz and 9420.08 Hz respectively. These values are in close agreement to the values calculated using (11) and (12), which are 9845.57 Hz and 9850.94 Hz for out-of-phase and in-phase modes respectively. The 3-DoF resonator system on each side of the proof mass is optimized such that the resonant frequency values of the resonator Set A and Set B perfectly match. At resonant
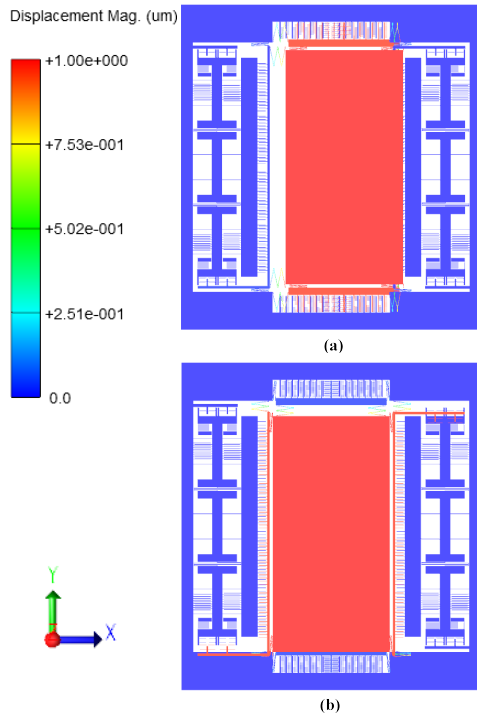
FIGURE 5. Mode shapes for the proposed design. (a) Drive mode of proof mass, (b) sense mode of proof mass, (c) out of phase mode of resonator system and (d) in phase mode of resonator system.
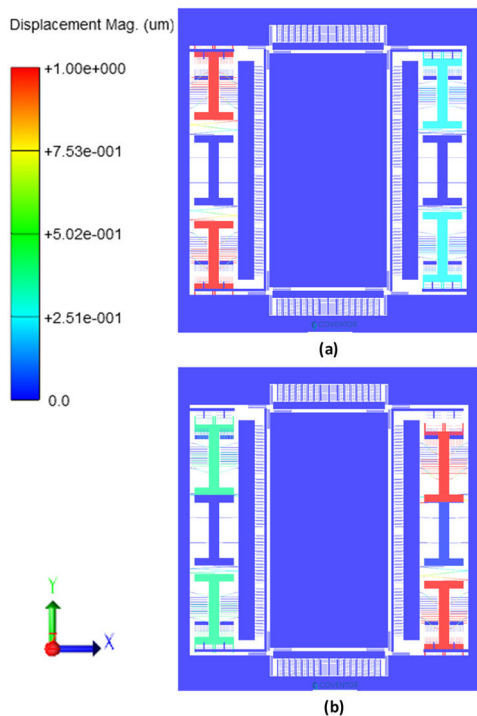

FIGURE 6. (a) out of phase mode of resonator system and (b) in phase mode of the resonator system.

frequency of 9416.48 Hz, the outer resonators in both resonator sets move out-of-phase while at resonant frequency of 9420.08 Hz the outer resonators in both sets move in the same

direction. The frequency difference between the out-of-phase and in-phase mode for the 3-DoF WCRs system is 3.6 Hz which is desired to avoid mode aliasing.

B. FREQUENCY RESPONSE ANALYSIS

The dynamic frequency response of the MEMS gyroscope is obtained by applying an electrostatic DC actuation voltage of 1 V superimposed on an AC voltage of 130 mV to the comb drive actuator attached to the proof mass. Under the influence of an actuation voltage and considering the effect of air damping, the proof mass oscillates with an amplitude of 0.1 μm at the drive axis resonant frequency. Fig. 7 shows the frequency response of the proof mass in drive and sense directions. The drive and sense mode resonant frequencies are initially mismatched by 60.3 Hz with a higher value for sense mode resonant frequency. The electrostatic frequency tuning plates in the proposed MEMS gyroscope design allow reducing the sense mode frequency by using the spring softening effect. Fig. 8 shows the effect of applying a DC voltage to the frequency tuning parallel plates on the sense mode resonant frequency of the MEMS gyroscope. The results show that as the applied voltage is increased the sense mode resonant frequency decreases and the drive and sense mode resonant frequencies are matched at a tuning voltage of 14.42 V.
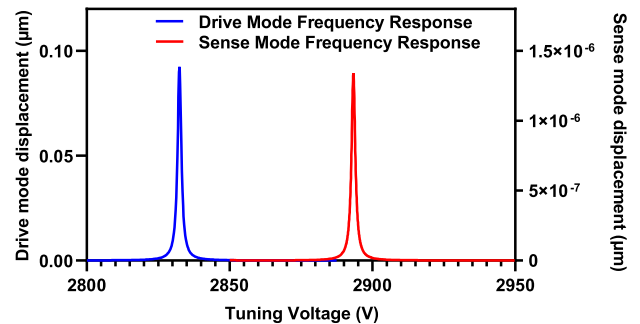

FIGURE 7. Drive and sense mode resonant frequency response of the MEMS gyroscope.

For frequency response analysis of the 3-DoF WCRs system, a DC voltage of 25 V and AC voltage of 15 mV, with a phase difference of 180 degrees, is applied to the electrostatic actuator attached to the outer resonators R_1 and R_3 in the resonator Set A. This excites the in-phase mode for the 3-DoF WCRs system. For this analysis, the input rotation to the MEMS gyroscope is not applied and thus the effect of stiffness perturbation in the resonator R_3 due to Coriolis force is zero. Fig. 9 shows the frequency response of the resonator R_1 and R_3 in the resonator Set A. The results show that at the in-phase damped resonant frequency of 8974.7 Hz, the oscillation amplitude of the resonators R_1 and R_3 is 0.135 μm and 0.138 μm respectively with an amplitude ratio of 0.97. Thus, at zero input perturbation, the amplitude ratio of the two resonators is not exactly one. This is due to the fact that the fixed electrodes for the resonator R_1 are anchored to the substrate whereas for the resonator R_3 they are attached to the
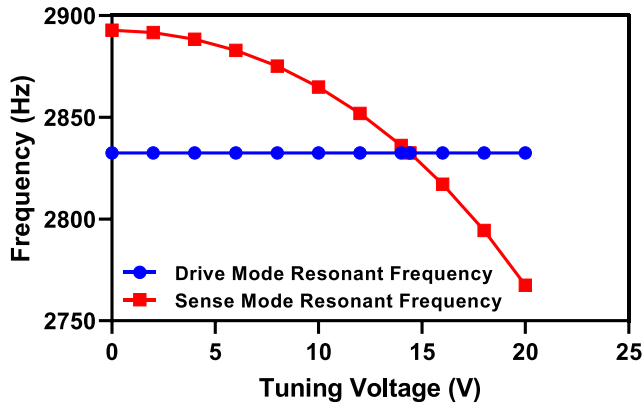
FIGURE 8. Effect of tuning voltage on the drive and sense mode resonant frequency of MEMS gyroscope.

FIGURE 10. Harmonic response for the resonator system showing the vibrational amplitudes for the resonator R_1 and R_3 after the application of angular rate.

sense decoupling frame. Due to this, after the initial biasing of the system, the electrostatic force on the resonator R_1 and resonator R_3 is different which results in an initial mode localization in the 3-DoF WCRs system even in the absence of an angular rotation applied to the MEMS gyroscope. However, this initial mode localization does not affect the performance of the MEMS gyroscope since only the equilibrium point has been slightly shifted.

Fig. 10 shows the frequency response for the resonators R_1 and R_3 in the resonator Set A with the application of an angular rate of 50 °/s to the MEMS gyroscope. This angular rate results in a normalized stiffness perturbation ($\Delta k/k_3$) of 0.0016 in the resonator R_3. The results show that with this stiffness perturbation and at the first out-of-phase resonant frequency, the oscillation amplitude of the resonator R_3 diminishes to 0.038 μm while that of resonator R_1 is 0.0879 μm due to mode localization. Similarly, at the second in-phase resonant frequency the oscillation amplitude of resonator R_3 increases to 0.163 μm, and that of R_1 decreases to 0.053 μm. The amplitude ratio $AR_{SET\ A} = y_1/y_3$ of the resonators, R_1 and R_3 in the resonator Set A at out-of-phase and the in-phase resonant frequency is thus 3.06 and 3.46 respectively.
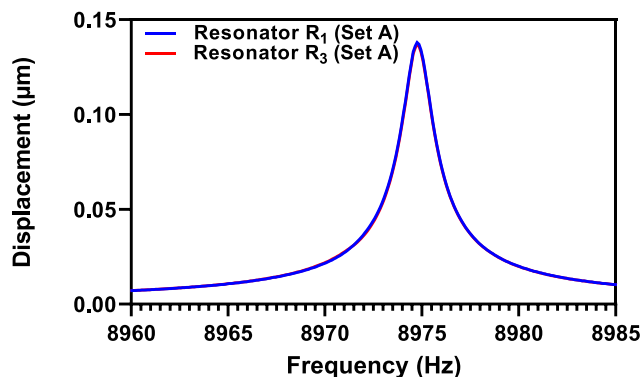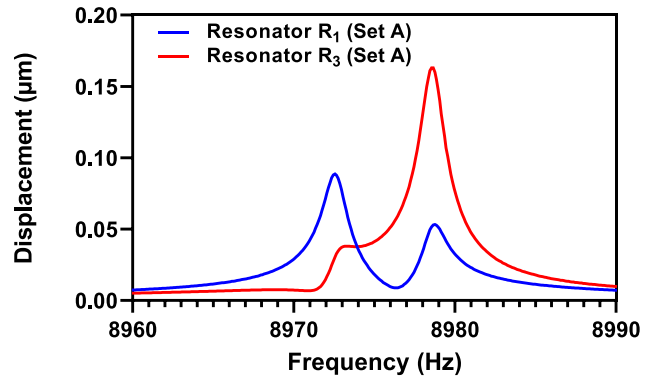
C. MODE ALIASING AND RESONANT FREQUENCY VARIATION ANALYSIS

For the 3-Dof WCR system, the quality factor affects the operational bandwidth of the system as at low pressures the in-phase and out-of-phase modes can overlap resulting in the mode aliasing effect where the modes are indistinguishable from one another. To avoid this effect the difference between the frequency values of the in-phase and out-of-phase resonant modes, Δf, must be greater than the frequency value of $2\Delta f_{3dB}$ [21]. For the resonator set A, the variation of resonant frequencies for the in phase and out of phase modes for an applied angular rate is shown in the Fig. 11. It shows that when no input angular rate is applied to the MEMS gyroscope the difference between the in-phase and out-of-phase modes is the smallest and it increases with an increase in the applied angular rate. So, the condition $\Delta f > 2\Delta f_{3dB}$ has to be satisfied at this point. The value of Δf at 0 °/s is 3.3 Hz whereas the value of Δf_{3dB} is 1.48 Hz twice of which is 2.96 Hz which is still less than the Δf value. The results in Fig. 11 show that for an angular rate of 50 °/s the frequency shift for the out-of-phase mode is 4.6 Hz which gives us a sensitivity of 92000 ppm/°/s. Whereas for the in-phase mode the frequency shift is 3.8 Hz which is almost twice that for the out of phase modes and gives us a sensitivity of 76000 ppm/°/s. This shows that if the system is to be operated based on the frequency shift instead of the amplitude ratio difference as an output metric for angular rate measurement, the mode of operation for the 3-DoF WCRs system should be the out-of-phase mode as it has better sensitivity.

D. AMPLITUDE RATIO AS THE OUTPUT METRIC

As discussed in section IV (B), the vibration amplitude of the resonators R_1 and R_3 in the 3-DoF WCRs Set A changes for an input perturbation in the resonator R_3 corresponding to input angular rate to the MEMS gyroscope. The input perturbation results in a decrease in the vibration amplitude of resonator R_3 while the vibration amplitude of resonator R_1 remains nearly constant for the out-of-phase mode of
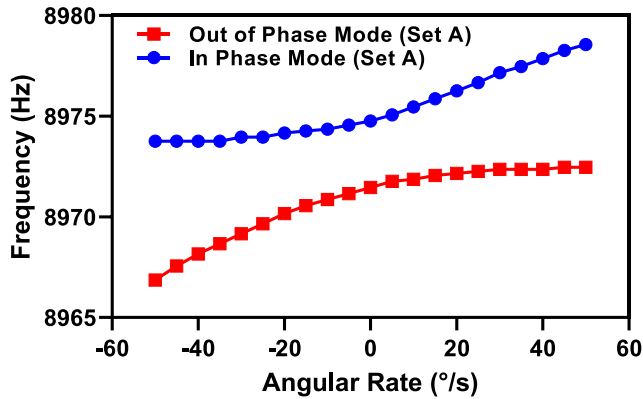

FIGURE 9. Harmonic response for the resonator system showing the vibrational amplitudes for the resonator R_1 and R_3.

FIGURE 11. Resonant frequency shift for in-phase and out-of-phase modes with the applied angular rate.
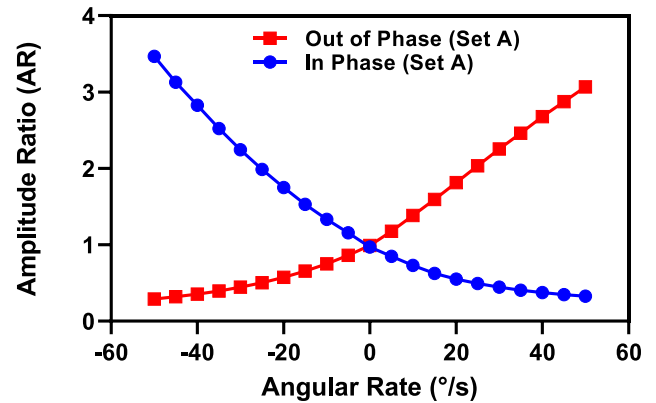

FIGURE 12. Amplitude ratios for in-phase and out-of-phase mode for an applied angular rate.

operation. The amplitude ratio of the resonators R_1 and R_3 can thus be used for the measurement of the input angular rate applied to the MEMS gyroscope. Fig. 12 shows the amplitude ratio (y_1/y_3) of the resonators R_1 and R_3 in the resonator Set A at out-of-phase and in-phase mode for an input angular rate in the range of -50 °/s to 50 °/s applied to the MEMS gyroscope. The results show that the amplitude ratio of the resonators for the in-phase mode is higher than the out-of-phase mode for an applied angular rate. For an angular rate of -50 °/s, the absolute amplitude ratio at in-phase mode is 3.46 which gives a relative amplitude ratio sensitivity (AR/°/$s \times 10^6$) value of 71200 ppm/°/s for the MEMS gyroscope. At out-of-phase mode, for an angular rate of -50 °/s, the absolute and relative amplitude ratio sensitivity values are 3.06 and 61200 ppm/°/s respectively. These results show that for the MEMS gyroscope design, the 3-DoF WCRs system should be operated in an in-phase mode to achieve better sensitivity.

E. AMPLITUDE RATIO DIFFERENCE AS THE OUTPUT METRIC

The results in Fig. 12 show that the amplitude ratio of the outer two resonators in a 3-DoF WCRs set can be used as an output metric for the angular rotation measurement only for the positive or negative value of the rotation. For the sensing of positive values of the angular rotation, the resonator should be excited in the out-of-phase mode and for the negative values of the angular rotation, the in-phase mode should be used. Moreover, for the low values of the input angular rotation, the amplitude ratio of the resonators is highly nonlinear. Since, in the proposed MEMS gyroscope design, two 3-DoF WCRs sets are mirrored on both sides of the proof mass and operate in a differential configuration, the amplitude ratio difference of the resonator Set A and Set B ($|AR_{SetA} - AR_{SetB}|$) can be used as an output metric for the MEMS gyroscope for sensing the angular rotation. Fig. 13 shows the amplitude ratio difference of the two 3-DoF WCRs sets for an input angular rate in the range of ±50 °/s. The results show that the ARD for the MEMS gyroscope is perfectly linear for the input angular rate in the range of ±50 °/s and the output response

is symmetric for the positive and negative values of the input rotation with the sensitivity value of 62830 ppm/°/s.

F. RESOLUTION AND DYNAMIC RANGE

The dynamic range of a MEMS gyroscope is an important performance parameter and is a deciding factor for the type of application for the device. For the proposed mode localization-based MEMS gyroscope, the upper limit of the measurable input rotation is decided by the oscillation amplitude of the resonators in the 3-DoF WCRs sets and the initial gap between the perturbation parallel plates. Fig. 14 shows the oscillation amplitude of the resonators R_3 in resonator Sets A and B. These resonators are electrostatically coupled to the perturbation parallel plates.

For the in-phase mode operation, at zero input rotation to the MEMS gyroscope, the oscillation amplitude of these two resonators is the same with a value of 0.13 μm. However, for a positive value of input rotation, the oscillation amplitude of the resonator R_3 in Set A increases to 0.165 μm for low values of input rotation and then remains nearly constant. The oscillation amplitude of resonator R_3 in the resonator Set B decreases non-linearly for the positive input rotations. The oscillation behavior of the two resonators in the resonator
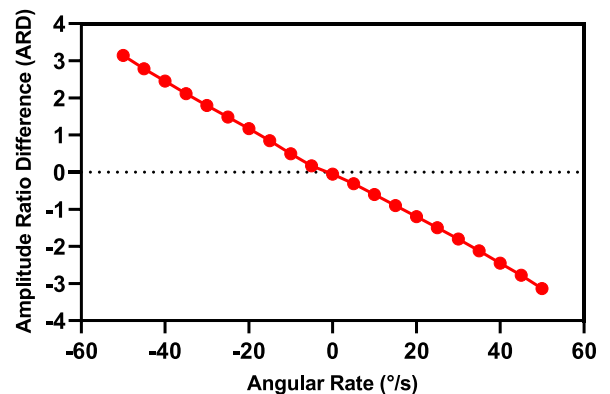

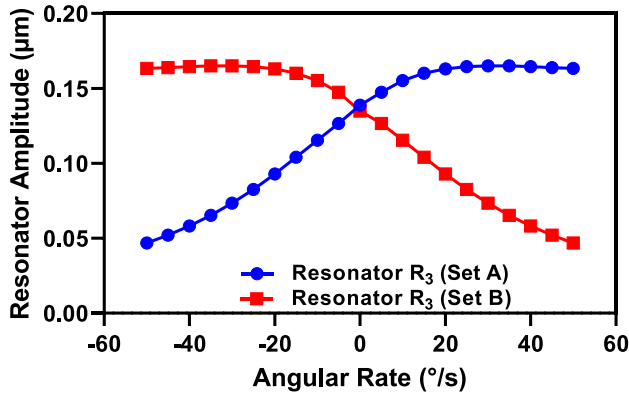**FIGURE 13.** Amplitude ratio difference for an input angular rate in the range of ±50 °/s.

FIGURE 14. Amplitudes of the perturbed resonators of Set A and B in in-phase mode for an applied angular rate.

Sets A and B follows an opposite trend for input rotation in the negative range. Thus, for the proposed MEMS gyroscope design, the maximum value of the oscillation amplitude for the resonators coupled to the parallel perturbation plates is lower than the 0.165 μm. The initial spacing between the parallel perturbation plates is 8 μm which decreases non-linearly with the displacement in the sense mass corresponding to the Coriolis force and hence input rotation. The phenomenon of pull-in plays an important role in deciding the maximum allowed displacement of the perturbation parallel plates. For parallel plate capacitors, the phenomenon of pull-in occurs if the moving parallel plates displace by one-third of the total gap, whereas, for an applied angular rate of 50 °/s the gap reduces to only 7.08 μm which is under the maximum allowed displacement. As the angular rate is increased beyond 50 °/s the phenomenon of non-linearity takes precedence over the pull-in phenomenon as the limiting factor for the maximum measurable angular rate. Fig. 15 shows the ARD values in a range of ±100 °/s whereas Fig. 16 shows the non-linearity in the output in a range from 0 to 100 °/s. The results show that the linearity of the output is affected by an increase in the applied angular rate which limits the effective measurement range of the device. So, a compromise between output linearity and the maximum measurable angular rate has to be made.

The lower limit of the measurement is just as important in deciding the application of the device as the upper limit. The lower limit or resolution of the device is dependent on the total noise floor of the device. In the case of the proposed system, this noise is the fluctuations in the amplitude of the resonators. The main source of noise in the 3dB bandwidth of the system, is the thermomechanical noise which is induced in the system due to the dynamic equilibrium between the surrounding thermal energy and the resonator's mechanical energy. Assuming Gaussian noise for the system and that the bandwidth is much less than the frequency, that is, $\Delta f_{3dB} \ll f_r$, The displacement due to noise is given by the expression [29];

$$x_r^{noise} = \sqrt{\frac{4k_b T \Delta f_{3dB} Q}{m_r \omega_r^3}} \qquad (21)$$

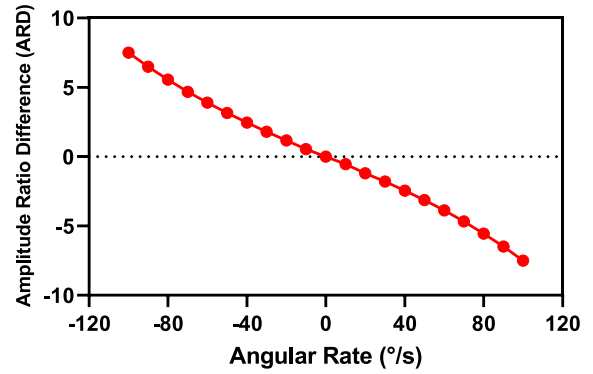**FIGURE 15.** Amplitude ratio difference for an angular rate of ±100 °/s.

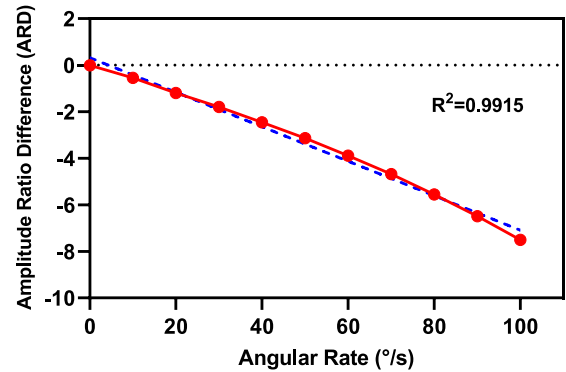**FIGURE 16.** Non-linearity in the output in the range of 0 to 100 °/s.

here T is the surrounding temperature, ω_r and m_r are the frequency and mass at resonance, and Q is the quality factor. The resolution for the system can be found by using this minimum displacement for the calculation of the minimum shift in the stiffness for the resonator R_3 for an applied angular rate. This can be found using the following equation;

$$\left(\frac{\Delta k}{k}\right)_{min} = 8\frac{k_c}{k}\sqrt{\frac{k_b T \Delta f_{3dB}}{2m_r \omega_r^3 x_r^2 Q}} \qquad (22)$$

Now the value of the resolution can be found by dividing this minimum stiffness change by the sensitivity of the device.

$$Resolution = \frac{(\Delta k/k)_{min}}{(\Delta k/k)/°/s} = 31.09 \times 10^{-6°}/s/\sqrt{Hz} \qquad (23)$$

This shows that the proposed mode-localization based resonant MEMS gyroscope design is capable of measuring an angular rate in the range of ±100 °/s with a resolution of 31.09 × 10-6 °/s. This measurement range makes the proposed MEMS gyroscope ideal for use in applications such as earth rate measurement, precision robotics, and local navigation of robots where an extremely small angular rotation must be detected. Table 2 shows the comparison of the proposed MEMS gyroscope design with the high resolution gyroscopes presented in the literature. The comparison shows that the using mode-localization in WCRs as a sensing mechanism for

TABLE 2. Comparison of the Proposed Mode Localization Based Resonant Gyroscope Design with the Designs Presented in the Literature.

Article	Technology	Resolution	Measurement Range
Ding et al. [22]	MEMS	0.0015 °/s	± 300 °/s
Ding et al. [30]	MEMS	0.0084 °/s	± 250 °/s
Schreiber et al. [31]	Ring Laser	0.12×10^{-6} °/s	-
Iozan et al. [17]	MEMS	0.06 °/s	± 100 °/s
This Work	MEMS	31.09×10^{-6} °/s	± 100 °/s

the input angular rotation allows achieving resolution much better than the conventional MEMS gyroscopes and is even comparable to the bulky ring laser gyroscopes.

V. CONCLUSION

In this paper, a new design approach for achieving high resolution MEMS gyroscopes is presented. The proposed design utilizes two sets of WCRs attached on either side of the proof mass system. The output metric for the system is the difference of the amplitude ratios of the two WCRs systems. In addition to ARD, the effect of input angular rate on the resonant frequency and AR change in WCRs is also presented for the proposed design, mode aliasing is avoided at zero input value as the value of Δf is 3.3 Hz whereas the value of $2\Delta f_{3dB}$ is 2.96 Hz which is less than Δf. There are two operational modes for the WCR systems, the in-phase mode and the out-of-phase mode. In the case of frequency shift, the output of the out-of-phase mode has a higher sensitivity with a value of 92000 ppm/°/s whereas for the in-phase mode it is 76000 ppm/°/s. The amplitude ratio for the WCRs at zero input is 0.97 which implies towards an initial mode-localization in the system. The amplitude ratio sensitivities of the proposed resonant MEMS gyroscope in the in-phase and out-of-phase modes are 712200 ppm/°/s and 61200 ppm/°/s respectively. Since the in-phase mode has a higher sensitivity value, it is selected as the preferred mode of operation. To avoid the non-linearity for low values of input angular rate, ARD is used as the output metric for the proposed system. The ARD sensitivity for the proposed design in the in-phase mode is 62830 ppm/°/s.

For the proposed MEMS gyroscope design, the output remains perfectly linear for an input range up to 50 °/s but as the applied angular rate is increased to 100 °/s the non-linearity increases but is still only 0.85%. The minimum measurable angular rate for the proposed resonant MEMS gyroscope is dependent on the thermal-mechanical noise in the system and is estimated to be equal to 31.09×10^{-6} °/s. This ultra-high resolution as well as a dynamic range of ±100 °/s makes the proposed design suitable for applications in the areas such as earth rate measurement and high precision robotics.

REFERENCES

[1] D. Yamane, T. Matsushima, T. Konishi, H. Toshiyoshi, K. Masu, and K. Machida, "A dual-axis MEMS capacitive inertial sensor with high-density proof mass," *Microsyst. Technol.*, vol. 22, no. 3, pp. 459–464, Mar. 2016, doi: 10.1007/s00542-015-2539-y.

[2] Q. Guo, W. H. Deng, O. Bebek, M. C. Cavusoglu, C. H. Mastrangelo, and D. J. Young, "Personal inertial navigation system assisted by MEMS ground reaction sensor array and interface ASIC for GPS-denied environment," *IEEE J. Solid-State Circuits*, vol. 53, no. 11, pp. 3039–3049, Nov. 2018, doi: 10.1109/jssc.2018.2868263.

[3] C. Acar, A. R. Schofield, A. A. Trusov, L. E. Costlow, and A. M. Shkel, "Environmentally robust MEMS vibratory gyroscopes for automotive applications," *IEEE Sensors J.*, vol. 9, no. 12, pp. 1895–1906, Dec. 2009, doi: 10.1109/jsen.2009.2026466.

[4] C. Eling, L. Klingbeil, and H. Kuhlmann, "Real-time single-frequency GPS/MEMS-IMU attitude determination of lightweight UAVs," *Sensors*, vol. 15, no. 10, pp. 26212–26235, Oct. 2015, doi: 10.3390/s151026212.

[5] A. Kos, S. Tomažič, and A. Umek, "Evaluation of smartphone inertial sensor performance for cross-platform mobile applications," *Sensors*, vol. 16, no. 4, p. 477, 2016, doi: 10.3390/s16040477.

[6] C. Acar and A. M. Shkel, "Inherently robust micromachined gyroscopes with 2-DOF sense-mode oscillator," *J. Microelectromech. Syst.*, vol. 15, no. 2, pp. 380–387, Apr. 2006, doi: 10.1109/jmems.2006.872224.

[7] K. Riaz, S. A. Bazaz, M. M. Saleem, and R. I. Shakoor, "Design, damping estimation and experimental characterization of decoupled 3-DoF robust MEMS gyroscope," *Sens. Actuators A, Phys.*, vol. 172, no. 2, pp. 523–532, Dec. 2011, doi: 10.1016/j.sna.2011.09.032.

[8] K. Sahin, E. Sahin, S. E. Alper, and T. Akin, "A wide-bandwidth and high-sensitivity robust microgyroscope," *J. Micromech. Microeng.*, vol. 19, no. 7, Jul. 2009, Art. no. 074004, doi: 10.1088/0960-1317/19/7/074004.

[9] M. M. Saleem and S. A. Bazaz, "Design and robustness analysis of structurally decoupled 3-DoF MEMS gyroscope in the presence of worst-case process tolerances," *Microsyst. Technol.*, vol. 17, no. 8, pp. 1381–1391, Aug. 2011, doi: 10.1007/s00542-011-1315-x.

[10] S. A. R. Bukhari, M. M. Saleem, U. S. Khan, A. Hamza, J. Iqbal, and R. I. Shakoor, "Microfabrication process-driven design, FEM analysis and system modeling of 3-DoF drive mode and 2-DoF sense mode thermally stable non-resonant MEMS gyroscope," *Micromachines*, vol. 11, no. 9, p. 862, Sep. 2020, doi: 10.3390/mi11090862.

[11] H. Cao, R. Xue, Q. Cai, J. Gao, R. Zhao, Y. Shi, K. Huang, X. Shao, andC. Shen, "Design and experiment for dual-mass MEMS gyroscope sensing closed-loop system," *IEEE Access*, vol. 8, pp. 48074–48087, 2020.

[12] J. Sun, S. Fan, H. Shi, W. Xing, C. Zhao, and C. Li, "Design and optimization of a resonant output frequency gyroscope for robust sensitivity and bandwidth performance," *Microsyst. Technol.*, vol. 22, no. 10, pp. 2565–2586, Oct. 2016, doi: 10.1007/s00542-015-2730-1.

[13] T. Hiller, Z. Pentek, J.-T. Liewald, A. Buhmann, and H. Roth, "Origins and mechanisms of bias instability noise in a three-axis mode-matched MEMS gyroscope," *J. Microelectromech. Syst.*, vol. 28, no. 4, pp. 586–596, Aug. 2019.

[14] W. Li, D. Xiao, X. Wu, J. Su, Z. Chen, Z. Hou, and X. Wang, "Enhanced temperature stability of sensitivity for MEMS gyroscope based on frequency mismatch control," *Microsyst. Technol.*, vol. 23, no. 8, pp. 3311–3317, Aug. 2017, doi: 10.1007/s00542-016-3114-x.

[15] S. Sonmezoglu, S. E. Alper, and T. Akin, "An automatically mode-matched MEMS gyroscope with wide and tunable bandwidth," *J. Microelectromech. Syst.*, vol. 23, no. 2, pp. 284–297, Apr. 2014, doi: 10.1109/jmems.2014.2299234.

[16] J. Jia, X. Ding, Y. Gao, and H. Li, "Automatic frequency tuning technology for dual-mass MEMS gyroscope based on a quadrature modulation signal," *Micromachines*, vol. 9, no. 10, p. 511, Oct. 2018, doi: 10.3390/mi9100511.

[17] L. I. Iozan, M. Kirkko-Jaakkola, J. Collin, J. Takala, and C. Rusu, "Using a MEMS gyroscope to measure the Earth's rotation for gyro-compassing applications," *Meas. Sci. Technol.*, vol. 23, no. 2, Feb. 2012, Art. no. 025005, doi: 10.1088/0957-0233/23/2/025005.

[18] J. Belfi, N. Beverini, F. Bosi, G. Carelli, D. Cuccato, G. De Luca, A. Di Virgilio, A. Gebauer, E. Maccioni, A. Ortolan, A. Porzio, G. Saccorotti, A. Simonelli, and G. Terreni, "Deep underground rotation measurements: GINGERino ring laser gyroscope in gran sasso," *Rev. Sci. Instrum.*, vol. 88, no. 3, Mar. 2017, Art. no. 034502, doi: 10.1063/1.4977051.

[19] D. F. Wang, K. Chatani, T. Ikehara, and R. Maeda, "Mode localization analysis and characterization in a 5-beam array of coupled nearly identical micromechanical resonators for ultra-sensitive mass detection and analyte identification," *Microsyst. Technol.*, vol. 18, no. 11, pp. 1923–1929, Nov. 2012, doi: 10.1007/s00542-012-1520-2.

[20] M. M. Saleem, S. Saghir, S. A. R. Bukhari, A. Hamza, R. I. Shakoor, and S. A. Bazaz, "A Low-g MEMS accelerometer with high sensitivity, low nonlinearity and large dynamic range based on mode-localization of 3-DoF weakly coupled resonators," *Micromachines*, vol. 12, no. 3, p. 310, Mar. 2021, doi: 10.3390/mi12030310.

[21] H. Zhang, J. Huang, W. Yuan, and H. Chang, "A high-sensitivity micromechanical electrometer based on mode localization of two degree-of-freedom weakly coupled resonators," *J. Microelectromech. Syst.*, vol. 25, no. 5, pp. 937–946, Oct. 2016, doi: 10.1109/jmems.2016.2598780.

[22] H. Ding, X. Liu, L. Lin, X. Chi, J. Cui, M. Kraft, Z. Yang, and G. Yan, "A high-resolution silicon-on-glass Z axis gyroscope operating at atmospheric pressure," *IEEE Sensors J.*, vol. 10, no. 6, pp. 1066–1074, Jun. 2010, doi: 10.1109/jsen.2010.2043669.

[23] C. Zhao, M. Pandit, G. Sobreviela, A. Mustafazade, S. Du, X. Zou, and A. Seshia, "On the noise optimization of resonant MEMS sensors utilizing vibration mode localization," *Appl. Phys. Lett.*, vol. 112, no. 19, May 2018, Art. no. 194103, doi: 10.1063/1.5025818.

[24] M. Manav, G. Reynen, M. Sharma, E. Cretu, and A. S. Phani, "Ultrasensitive resonant MEMS transducers with tuneable coupling," *J. Micromech. Microeng.*, vol. 24, no. 5, May 2014, Art. no. 055005, doi: 10.1088/0960-1317/24/5/055005.

[25] C. Zhao, G. S. Wood, J. Xie, H. Chang, S. H. Pu, and M. Kraft, "A three degree-of-freedom weakly coupled resonator sensor with enhanced stiffness sensitivity," *J. Microelectromech. Syst.*, vol. 25, no. 1, pp. 38–51, Feb. 2016, doi: 10.1109/jmems.2015.2490204.

[26] M. Pandit, C. Zhao, G. Sobreviela, X. Zou, and A. Seshia, "A high resolution differential mode-localized MEMS accelerometer," *J. Microelectromech. Syst.*, vol. 28, no. 5, pp. 782–789, Oct. 2019, doi: 10.1109/jmems.2019.2926651.

[27] *SOIMUMPs Design Handbook*, MEMSCAP Inc, Durham, NC, USA, 2011, pp. 2002–2011.

[28] C. Acar and A. Shkel, *MEMS Vibratory Gyroscopes*. New York, NY, USA: Springer, 2008, p. 116.

[29] R. Perelló-Roig, J. Verd, S. Bota, and J. Segura, "Thermomechanical noise characterization in fully monolithic CMOS-MEMS resonators," *Sensors*, vol. 18, no. 9, p. 3124, Sep. 2018, doi: 10.3390/s18093124.

[30] H. Ding, "A bulk micromachined z-axis single crystal silicon gyroscope for commercial applications," in *Proc. 3rd IEEE Int. Conf. Nano/Micro Eng. Mol. Syst.*, Jan. 2008, pp. 1039–1042. [Online]. Available: https://ieeexplore.ieee.org/abstract/document/4484497?casa_token=ZrFo3FrTDSgAAAAA:I7uxJKOB1-RvGDDNgOotm2CbbEao8wuprVvqP1VkDs4wA6efKZlzekYKYHa_uW55_A7s-24vCA4C

[31] K. U. Schreiber, T. Klügel, J.-P.-R. Wells, R. B. Hurst, and A. Gebauer, "How to detect the chandler and the annual wobble of the Earth with a large ring laser gyroscope," *Phys. Rev. Lett.*, vol. 107, no. 17, Oct. 2011, Art. no. 173904, doi: 10.1103/physrevlett.107.173904.

MUHAMMAD MUBASHER SALEEM (Member, IEEE) received the B.S. degree in electrical engineering from the University of Engineering and Technology, Lahore, Pakistan, in 2008, the M.S. degree in electronics engineering from the GIK Institute of Engineering Sciences and Technology, Topi, Pakistan, in 2010, and the Ph.D. degree in mechanical engineering, with research thesis on MEMS design and development, from the Politecnico di Torino, Italy, in 2015. He is currently working as an Assistant Professor with the National University of Sciences and Technology, Islamabad, Pakistan. He has published over 50 research publications on MEMS devices in reputed journals and conferences. His current research interests include development of MEMS inertial sensors, RF-MEMS, micro/nanorobotics, and MEMS reliability. He was awarded quality research award for year 2015, for his Ph.D. thesis on MEMS devices by the Polytecnico di Torino.

AMIR HAMZA received the bachelor's degree in mechatronics engineering from the National University of Sciences and Technology, Pakistan, in 2005, the M.S. degree in mechanical engineering from Seoul National University, South Korea, and the Ph.D. degree in mechanical engineering from the King Fahd University of Petroleum and Minerals, Saudi Arabia. He is currently working as an Assistant Professor with the Department of Mechatronics Engineering, National University of Sciences and Technology. He is also the Head of the Mechatronics Engineering Department.

SHAFAAT AHMED BAZAZ graduated in avionics engineering from the College of Aeronautical Engineering, Risalpur, in 1989. He received the master's degree from the Université de Franche Comté, Besançon, France, in 1994, and the Ph.D. degree from the Institut National des Sciences Appliquées (INSA), Toulouse, France, in 1998.

He has been working in the field of VLSI & MEMS for more than 20 years. From 1999 to 2000, he worked as a Research Assistant Professor with the Technical University of Denmark (DTU). There, he supervised CAD for MEMS project funded by the Denmark Technical Research Council. From 2000 to 2006, he worked in CMC Microsystems in Canada as a Senior Staff Scientist in microsystem engineering. He has developed design kits and design flows for many MEMS and micro-fluidic technologies.

SYED ALI RAZA BUKHARI received the B.E. degree in mechatronics engineering from Air University, Islamabad, Pakistan, in 2018, and the M.S. degree in mechatronics engineering from the National University of Sciences and Technology, Islamabad. He is currently working as a Design Engineer in an industry funded collaborative project at the Department of Mechatronics Engineering, National University of Sciences and Technology. His main research interests include design and analytical modeling of MEMS sensors and actuators with particular focus on high performance inertial sensors.

● ● ●